Effective Diffusion Coefficients in Square Arrays of Filament Bundles

Faye Transvalidou and Stratis V. Sotirchos
Dept. of Chemical Engineering, University of Rochester, Rochester, NY 14627

The effects of the polydispersity of the characteristic diffusion length of the pore space of fibrous media on the effective diffusion coefficients of gases are studied by investigating the problem of gaseous diffusion in the Knudsen, transition, and bulk regimes in square arrays of filament bundles, of cylindrical cross section, consisting of unidirectional, freely overlapping cylindrical filaments. Effective diffusion coefficients are computed using a stochastic simulation method based on the computation of the mean square displacement of a large number of molecules (random walkers) diffusing in the pore space. The dependence of effective diffusivity on filament to bundle radius ratio, intrabundle porosity, interbundle porosity, and Knudsen number is investigated in detail. The computed diffusivities are compared to the predictions of analytical or semianalytical formulas based on expressions derived in the literature for two-phase media or bidisperse pore structures.

Introduction

Knowledge of the effective transport properties of multiphase media (e.g., diffusion coefficient, thermal conductivity, electrical conductivity, and magnetic permeability) is required for the study and analysis of almost all processes in which such materials are encountered. Numerous investigations have thus been conducted on the dependence of the effective transport properties on the structure of multiphase media, and most of them have dealt with the most frequently encountered case of two-phase media, of which porous materials are the most typical example. Among the problems lending themselves to theoretical treatment are those where one of the phases is dispersed within the other in the form of regular arrays (i.e., cubic, square, hexagonal) of simple geometric bodies (e.g., cylinders and spheres). Maxwell (1881) was the first to consider the transport problem in a material consisting of spheres embedded in a matrix of different conductivity, and the analogous problem for a square array of cylinders was studied by Lord Rayleigh (1892). The last problem was revisited by Perrins et al. (1979), who also considered hexagonal arrays of cylinders and various conductivity ratios for the cylinder–matrix pair. Their work was extended by Milton et al. (1981) to square arrays of partially overlapping cylinders.

Correspondence concerning this article should be addressed to S. V. Sotirchos.

Most multiphase (composite) materials, natural or manmade, exhibit some randomness in their structure, and therefore they can be better represented by disordered structures. As in the case of ordered structures, the most commonly followed approach for finding the effective transport coefficients of random structures consists of determining the microscopic potential (concentration in the case of diffusion) field in a unit cell, using it to compute the average flux, and extracting the effective transport coefficient from its definition. Even for the simplest random structures, use of numerical methods is required for determining the microscopic potential field by solving the transport equations in each phase along with appropriate boundary conditions at the interfaces and at the boundaries of the unit cell. Analytical results can be obtained by using approximations to the microscopic potential field, and this is the basis of some of the methods used to determine bounds for the effective transport properties of random structures from multipoint probability functions (Beran, 1968; Hashin and Shtrikman, 1962; Torquato, 1985). Methods used to study transport in porous media are reviewed by Sahimi (1995).

Effective transport coefficients can also be determined by using another approach based on exploiting the relationship that exists between a random-walk process and the solution of the diffusion equation (Einstein, 1926; Chandrasekhar,

1943). In this approach, the effective transport coefficient or the components of the effective transport coefficient tensor (for anisotropic structures) can be extracted from the mean square displacement of a large number of random walkers, for mean square displacements much larger than the characteristic phase length. Compared to methods based on the determination of the microscopic potential field, the random walk method has the advantage that it can also be employed when transport in each phase cannot be treated as a continuum process. It can thus be applied to studying gaseous diffusion in the Knudsen or transition regime, where the mean free path of the diffusing molecules is much larger than, or comparable to, the average wall-to-wall distance (pore size), and as a result, molecule–wall collisions outnumber or are as frequent as those between molecules.

Tomadakis and Sotirchos (1991a,b, 1993a–e) used the random-walk method to study diffusive transport in randomly overlapping fibrous structures for various orientation distributions: unidirectional (fibers parallel to a line), bidirectional (fibers parallel to a plane), and tridirectional (fibers randomly oriented in the 3-dimensional space). For the case of unidirectional fibers, they also investigated the situation (Tomadakis and Sotirchos, 1993b) in which the fibers exist in a nonoverlapping or partially overlapping arrangement. Fibrous materials are encountered in many applications, ranging from filtration and other separation processes to fabrication of ceramic, carbon, or metal matrix composites. A particular application that requires knowledge of the effective diffusion coefficients of gases in the interior of a fibrous medium is the process of chemical-vapor infiltration, in which fiber-reinforced composites are fabricated by depositing solid material within the pore space of a fibrous preform using a gas–solid reaction process (Naslain, 1992; Sotirchos, 1991).

The effective diffusivities that were computed by Tomadakis and Sotirchos (1991a,b, 1993a–e) and by other investigators (Melkote and Jensen, 1992) for fibrous media and the various bounds that were formulated by various investigators on the transport properties and effective diffusivities are for the case where the fibers are distributed uniformly in the structure of the fibrous medium, like the unidirectional structure of nonoverlapping fibers shown in Figure 1a. However, the fibrous media that are employed in many practical applications possess more than one level of structural organization. Such structures are exemplified by woven fibrous media, where the fibers are grouped into threads (straight or twisted bundles), which in turn are organized into cloth according to some 2- or 3-dimensional pattern. An example of a fibrous structure possessing two levels of structural organization is shown in Figure 1b. This structure has been obtained by rearranging the fibers of the homogeneous structure of Figure 1a into four bundles. Since the same number of nonoverlapping filaments is encountered in both structures in Figure 1, their macroscopic properties (surface area and porosity) are the same. However, this is not expected to be the case for the diffusion coefficients of gases in their pore space, especially in the Knudsen and transition diffusion regimes, where the effective diffusion coefficient is influenced not only by the relative spatial arrangement and orientation of the gas–solid interfaces but by the average wall-to-wall distances as well.

A great variety of thread types and weave patterns is exhibited by the fibrous woven media that are used in applications

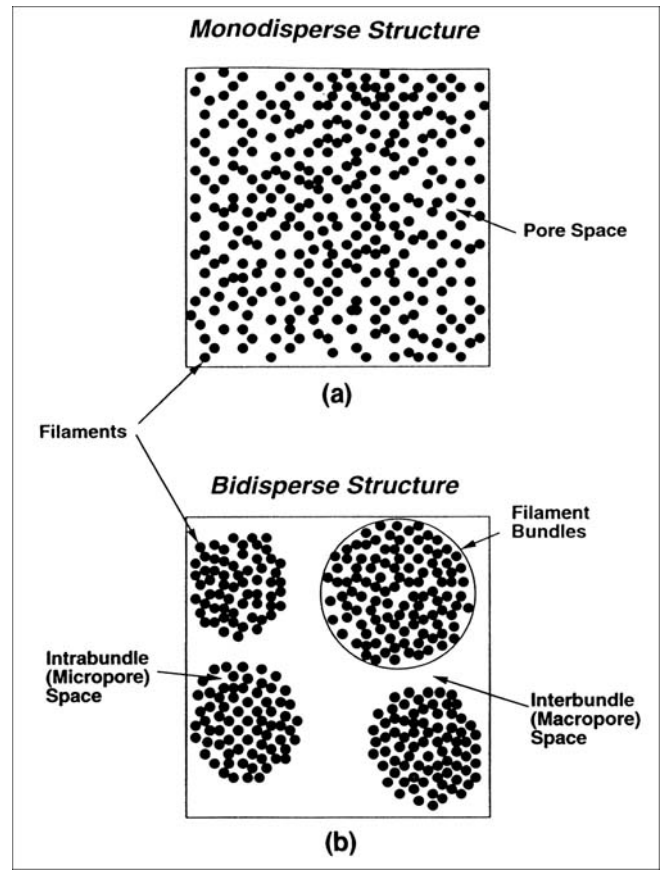

Figure 1. Example of a bidisperse porous medium of fibrous structure (b) resulting from a homogeneous structure through rearrangement of the fibers.

(Ko, 1989; McAllister and Lachman, 1983). As a first step toward understanding the effect of local microstructural organization in fibrous porous media on their macroscopic (effective) transport properties, we present in this study results on the effective diffusivity of gases in the bulk, transition, and Knudsen diffusion regimes in a square array of unidirectional filament bundles of circular cross section, each bundle consisting of untwisted, randomly overlapping filaments. A Monte Carlo simulation method based on a random walk scheme similar to that used in studies by Tomadakis and Sotirchos (1993a) is employed for the computations. Effective diffusivities (or, equivalently, tortuosities) are presented for a square array of solid (impermeable) cylinders. For the case in which solid deposition or a gas–solid reaction is used to densify a preform consisting of filament bundles, these results are of interest in the late stages of densification after all open accessible space in the bundles is eliminated and the bundles behave with regard to diffusion as solid cylinders.

Unit Cell Construction and Structural Properties

In the literature of woven fabrics and other fibrous materials, the terms yarn, thread, fiber, and filament are often used almost indistinguishably. Following terminology suggested by Schwartz (1992), in this study we employ the term *filament* to

denote a solid, individual, continuous fiber of circular cross section, with very large aspect (length-to-diameter) ratio. For most industrial applications, the radius of a filament, which we will represent by r_f, is in the 1–20 μm range. A *bundle* is an assembly of circular cross section consisting of many (from a few hundred to a few thousand) untwisted, unidirectional filaments that are densely packed. Its radius, denoted by r_b, may vary depending on the number of filaments, their size, and the packing density.

We define as interbundle (or macropore) space the void space available for diffusion between the bundles and as intrabundle (or micropore) space the void space within each bundle. This use of the macropores and micropores terms should not be confused with their prevailing use in the porous media literature, where micropores are generally pores of size less than 20 Å and macropores are pores larger than 1,000 Å. The intrabundle porosity (or microporosity) is denoted by ϵ_μ, and refers to the void space per unit of bundle volume, whereas the interbundle porosity (or macroporosity) denoted by ϵ_M refers to the volume of interbundle space per unit of cell volume. The filament (micropore) surface area is denoted by S_μ and defined per unit of bundle volume, while the bundle surface area, the area of the imaginary circular boundaries of the bundles, is expressed per unit of total volume and represented by S_M.

Let ϵ and S be the total porosity and total internal surface area of the structure of filament bundles. Assuming that the statistical properties of the bundles (porosity and surface area) are the same everywhere within their structure—the average porosity and internal surface area at the periphery differ from those in the interior of the bundles—the following equations may be used to relate the total porosity and internal surface area to the intrabundle and interbundle values:

$$\epsilon = \epsilon_M + (1-\epsilon_M)\epsilon_\mu \tag{1}$$

$$S = (1-\epsilon_M)S_\mu. \tag{2}$$

If ℓ_b is the length of bundles per unit of total volume, the macroporosity and the internal surface area of the bundles are given, for nonoverlapping bundles, by the formulas

$$\epsilon_M = 1 - \ell_b \pi r_b^2 \tag{3}$$

$$S_M = 2\,\ell_b \pi r_b. \tag{4}$$

For one bundle per unit cell of side a, as in the present application, Eqs. 3 and 4 become

$$\epsilon_M = 1 - \pi\left(\frac{r_b}{a}\right)^2 \tag{5}$$

$$S_M = 2\pi\left(\frac{r_b}{a^2}\right). \tag{6}$$

Needless to say, these equations are valid only above the porosity limit ($\epsilon_M = 1 - \pi(r_b/a)^2 = 0.2146\cdots$) at which a close-packed structure is obtained. At porosities below this value, ϵ_M and S_M are given by the equations

$$\epsilon_M = 1 - 2\sqrt{\left(\frac{r_b}{a}\right)^2 - \left(\frac{1}{2}\right)^2} - \left(\frac{r_b}{a}\right)^2(\pi - 4\theta) \tag{7}$$

$$S_M = \frac{2r_b}{a^2}(\pi - 4\theta) \tag{8}$$

with

$$\theta = \arccos\left(\frac{a}{2r_b}\right).$$

The bundles are assumed to consist of randomly overlapping filaments. If ℓ_f is the length of filament axes per unit of bundle volume, it can be shown (Sotirchos, 1987) that the bundle properties can be found from the equations

$$\epsilon_\mu = \exp\left(-\pi\,\ell_f r_f^2\right) \tag{9}$$

$$S_\mu = 2\pi\,\ell_f r_f \epsilon_\mu. \tag{10}$$

We will use the mean random chord length to characterize the average wall-to-wall distance in each of the three structures [microstructure (intrabundle space), macrostructure (interbundle space), and overall structure]. The mean random chord length is the mean of the random chords that are generated in the pore space by placing the porous medium in a random field of lines, and it corresponds to the pore diameter in a population of uniformly sized cylindrical pores that has the same porosity and surface area as the porous medium. For a porous medium of porosity ϵ and surface area S, the mean chord length $\bar{d}$ is found from the equation

$$\bar{d} = \frac{4\epsilon}{S} \tag{11}$$

Application of Eq. 11 to the macrostructure, microstructure, and overall structure yields the equations

$$\frac{\bar{d}_M}{a} \equiv \frac{4\epsilon_M}{S_M a} = \frac{2\epsilon_M}{\sqrt{\pi(1-\epsilon_M)}} \tag{12}$$

$$\frac{\bar{d}_\mu}{a} \equiv \frac{4\epsilon_\mu}{S_\mu a} = \left(\frac{-2}{\ln\epsilon}\right)\left(\frac{r_f}{a}\right) \tag{13}$$

$$\frac{\bar{d}}{a} \equiv \frac{4\epsilon}{Sa} = \bar{d}_\mu\left(1 + \frac{\epsilon_M}{(1-\epsilon_M)\epsilon_\mu}\right). \tag{14}$$

Equations 1–14 give the expected values of the structural properties, that is, the average of a large number of realizations. The unit cell of each realization is chosen to be of cubic shape with a single bundle placed at its center perpendicularly to a pair of its faces. For a given macroporosity, Eq. 5 is used to determine the bundle radius, r_b. The positions of the filaments in the bundle are generated by selecting random points on the base of the cubic unit cell that lie within a circle of radius $(r_b - r_f)$ from its center. $\pi(r_b - r_f)^2\,\ell_f$ filaments are introduced in each bundle, with ℓ_f found from the values of microporosity and filament size using Eq. 9. All fila-

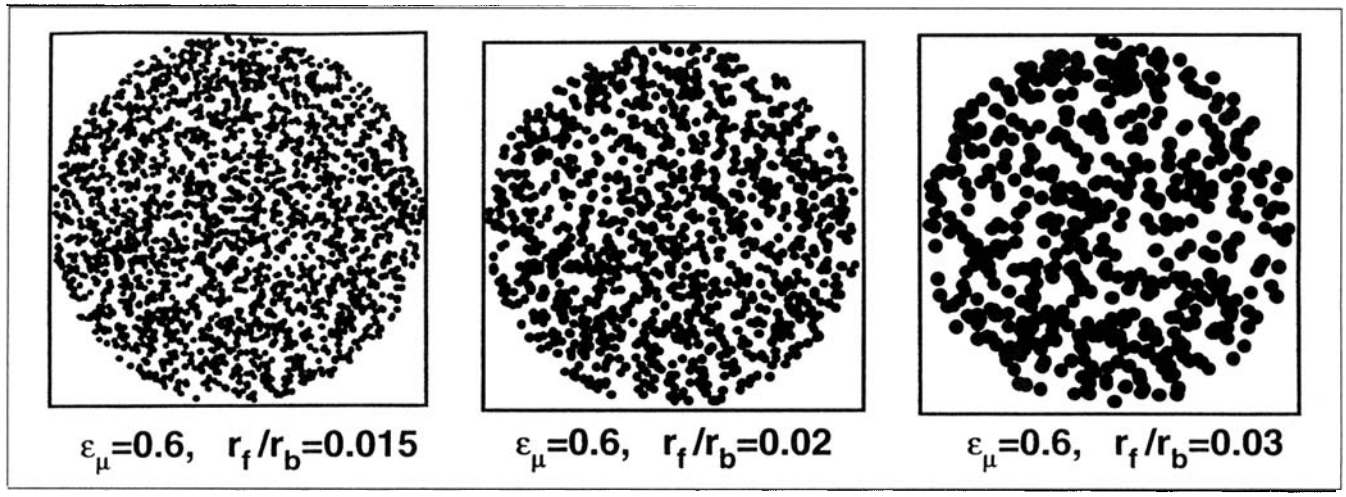

Figure 2. Cross-section of unit-cells with $\epsilon_M = 0.2146$ and different filament to bundle radius ratios.

ments generated by this construction procedure lie wholly within the bundle if $r_b \leq a/2$. For bundle diameters larger than the unit cell size, that is, for overlapping bundles, periodic boundary conditions are employed at opposite faces of unit cell as the positions of the fibers are chosen.

In the construction of the structures used to obtain Knudsen and transition-regime results, the r_f/r_b ratio was set equal to 0.015, 0.02, or 0.03. In order to save computational time in the bulk diffusion regime, the number of filaments in the bundle was kept approximately constant (around 900) and the r_f/r_b ratio was varied to achieve the desired microporosity. This could be done because in the bulk regime the effective diffusivity depends only on the interbundle and intrabundle porosities (for a relatively large number of filaments in the bundle). Once a certain structure was constructed, structures of larger or smaller macroporosity with the same number of filaments per bundle and the same r_f/r_b ratio could be obtained by simply decreasing or increasing the filament and bundle radii by the same factor. The average porosity in the annulus of thickness r_f at the edge of the bundle is higher than the target value ϵ_μ, but for small r_f/r_b ratios—as is the case in practice—this region corresponds to a very small fraction of the total intrabundle space. The cross section of a unit cell constructed by the preceding procedure is shown in Figure 2.

Mean Square Displacement Method

Effective diffusivities are computed using the mean square displacement, $\langle \xi^2 \rangle$, of a large number (between 800 and 1,000) of molecules. The molecules are introduced randomly in the void space, where they are allowed to travel for a sufficiently long time τ, performing a random walk. Details on the method are given by Burganos and Sotirchos (1989) and Tomadakis and Sotirchos (1993a), and thus only its salient points will be presented here.

The equation relating $\langle \xi^2 \rangle$, τ, and the effective diffusivity is extracted from the formula for the displacement probability of the molecules in the porous medium, which is in turn derived from the solution of the diffusion equation (Fick's second law). The final expressions are

$$D_e = \frac{\langle \xi^2 \rangle}{6\tau} \tag{15}$$

$$D_{e,xy \text{ or } z} = \frac{\langle \xi^2_{x,y \text{ or } z} \rangle}{2\tau}, \tag{16}$$

where subscripts x, y, or z denote the effective diffusivity in the x, y, or z direction and D_e is the orientationally averaged effective diffusivity, equal to one-third of the trace of the effective diffusivity tensor.

The molecules are assumed to travel, undergoing diffuse reflections on the surface of filaments (according to the cosine law) and random intermolecular collisions. Exponential distribution of free paths is used between intermolecular collisions. At selected instants, each molecule's square displacement from its initial position is stored, and these results are used to compute the mean square displacements for these travel times after all molecules complete their travel. Mirror boundary conditions are employed to extend the unit cell to the whole 3-dimensional space. Needless to say, the types of boundary conditions become an issue only when the bundles overlap. To save computational time, discretization of the unit cell and of the random paths is employed, using a scheme described in Tomadakis and Sotirchos (1993a).

Tortuosity factors are calculated using the equations:

$$\frac{D_e}{D(\bar{l})} = \frac{\epsilon}{\eta} \tag{17}$$

$$\frac{D_{e,xy \text{ or } z}}{D(\bar{l})} = \frac{\epsilon}{\eta_{x,y \text{ or } z}} \tag{18}$$

$$D(\bar{l}) = \frac{1}{3}\bar{l}\bar{v} \tag{19}$$

$$\bar{l} = \left(\frac{1}{\bar{\lambda}} + \frac{1}{\bar{d}}\right)^{-1} \tag{20}$$

where $D(\bar{l})$, the reference diffusivity, is equal to the Knudsen diffusivity in a pore of diameter $\bar{d}$ in the Knudsen regime ($(1/3)\bar{d}\bar{v}$), and to the self-diffusion coefficient of the gas

$((1/3)\bar{\lambda}\bar{v})$ in the bulk diffusion regime, $\eta_{x,y \text{ or } z}$ are the directional tortuosity factors, and η is the tortuosity corresponding to the orientationally averaged effective diffusivity. The effective diffusivities (or tortuosities) perpendicularly to the bundles (x and y direction) are equal to each other because of the isotropy of the fibrous structure on the (x,y) plane. It should be noted that $\bar{l}$ is equal to the mean length of the chords that are formed in the pore space when the porous medium is exposed to a field of random segments having mean length $\bar{\lambda}$ (Kellerer, 1971; Tomadakis and Sotirchos, 1993e), which in turn equals the average path between collisions of the molecule diffusing in the pore space.

Knudsen Diffusion in Polydisperse Structures

Before proceeding with the presentation and discussion of the results, we briefly discuss our definition of Knudsen, transition, and bulk regime diffusivity for the structures we examine in this study, which are typical examples of bidisperse porous structures.

The three diffusion regimes are usually defined on the basis of the ratio of the mean free path in the gas phase, $\bar{\lambda}$, to the mean random chord of the structure, $\bar{d}$, which is referred to as the Knudsen number, Kn, of the porous medium ($Kn = \bar{\lambda}/\bar{d}$). A large Knudsen number characterizes a diffusion process where collisions with the wall offer the most resistance to the diffusive flow. In the opposite case of bulk diffusion, intermolecular collisions influence more strongly the effective diffusivity. The definition of Knudsen number is simple and provides a sufficient characterization of the dominant diffusion mechanism for monodisperse (homogeneous) structures, characterized by a single length scale. However, for polydisperse (inhomogeneous) porous structures, one has to take into account that the length scales associated with diffusion in different regions of the pore space (intrabundle and interbundle space for the present problem) may differ significantly from each other.

For a polydisperse structure, diffusion occurs in the Knudsen diffusion regime only if the mean free path is much larger than the largest characteristic length encountered in the structure. On the other hand, bulk diffusion requires that the smallest characteristic length be much larger than the mean free path of the diffusing molecules. In all other cases, the overall process must be characterized as transition regime diffusion even though transport in some of the regions of the polydisperse medium may be governed by molecule–molecule collisions (bulk diffusion) or molecule–wall collisions (Knudsen diffusion).

On the basis of the mean chord length (Eq. 11), three characteristic lengths were defined for the bidisperse structure we examine here in Eqs. 12–14. The micropore characteristic length, $\bar{d}_\mu$, is typically much smaller than the interbundle (macropore) average pore diameter, $\bar{d}_M$. The overall characteristic length $\bar{d}$ lies between these two sizes, but it is in general (see Eq. 14) of the same order of magnitude as the micropore size and converges to it as the interbundle porosity goes to zero. Depending on the relative magnitudes of $\bar{d}_\mu$ and $\bar{d}_M$ and the value of $\bar{\lambda}$, four intermediate transition regimes can be distinguished in a bidisperse structure in addition to the bulk and Knudsen regimes. All six cases are listed in Table 1 in terms of the dominant diffusion mechanism prevailing in the macropore and micropore regions.

Table 1. Possible Combinations of Diffusion Mechanisms in the Macropore and Micropore Regions and the Resulting Characterization of the Diffusion Process in the Bidisperse Medium

Diffusion in Macropores	Diffusion in Micropores	Overall Process
Knudsen	Knudsen	Knudsen
Transition	Knudsen	Transition
Transition	Transition	Transition
Bulk	Knudsen	Transition
Bulk	Transition	Transition
Bulk	Bulk	Bulk

In order to characterize the overall transport process as Knudsen diffusion, we have to ensure that the mean free path $\bar{\lambda}$ employed in our simulations is such that molecule–wall collisions outnumber intermolecular collisions by a few orders of magnitude. It can be shown (Tomadakis and Sotirchos, 1993a) that the ratio of intermolecular to molecule–wall collisions is equal to $1/Kn$. We thus chose to work in the Knudsen regime with a value of $\bar{\lambda}$ that would yield $Kn_M = 100$. In accordance with the preceding discussion, we based our choice on the mean intercept length of the interbundle space to ensure that diffusion occurs in the Knudsen regime everywhere. For the bulk diffusion, we chose the mean free path $\bar{\lambda}$ to be approximately fifty times smaller than the intrabundle mean intercept length $\bar{d}_\mu$, (i.e., $Kn_\mu = 0.02$) to ensure that intermolecular collisions would be much more frequent than collisions with the solid walls in both regions (interbundle and intrabundle). This choice was based on the observation made by Tomadakis and Sotirchos (1993a) that for $Kn < 0.02$ the tortuosities for random fibrous structures calculated from simulations varied insignificantly with the Knudsen number. The transition regime results we present were based on the overall Knudsen number and were obtained for $Kn = 100$. For the r_f/r_b ratios we employed in our computations, this choice leads to Knudsen diffusion in the micropores and transition diffusion in the interbundle space (second case in Table 1).

Results and Discussion

Square array of solid bundles

In this section we present effective dimensionless diffusivities and tortuosities as functions of porosity for an infinitely extended square array of solid cylinders, that is, for the interbundle space of a structure of fiber bundles. The unit cell used in the simulation scheme in this case simply consists of a single cylinder placed at the center of a cube perpendicularly to a pair of opposite faces. As we pointed out earlier, this problem arises at the late stages of the densification of a fibrous medium by a gas–solid reaction process after all accessible intrabundle void areas are filled with solid material.

Results for the effective directional diffusivities are presented in Figures 3 and 4 for Knudsen numbers 0.02, 1, and 100 corresponding to the three diffusion regimes (bulk, transition, and Knudsen). The data points shown in the figure were obtained for 800 molecules, each covering a total travel distance of about 3,000 unit cell sides. More than one data points are shown at some porosities, and the differences among these data points are representative of the differences

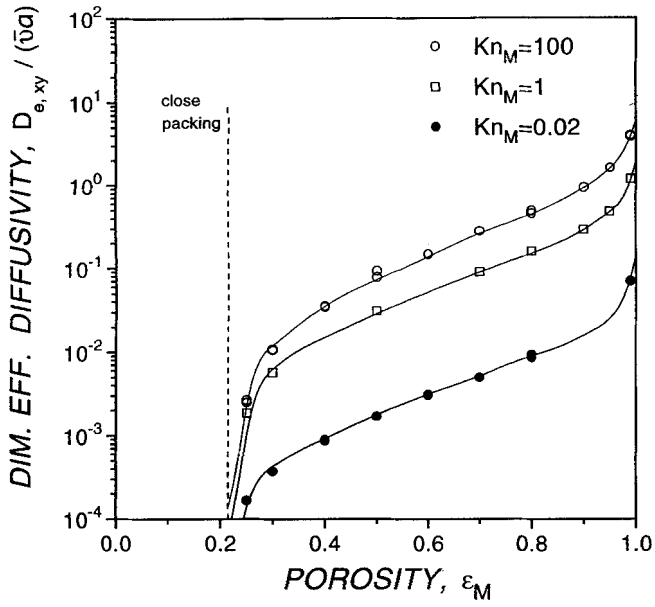

Figure 3. Variation of the transverse effective diffusivity with the porosity for a square array of solid cylinders.

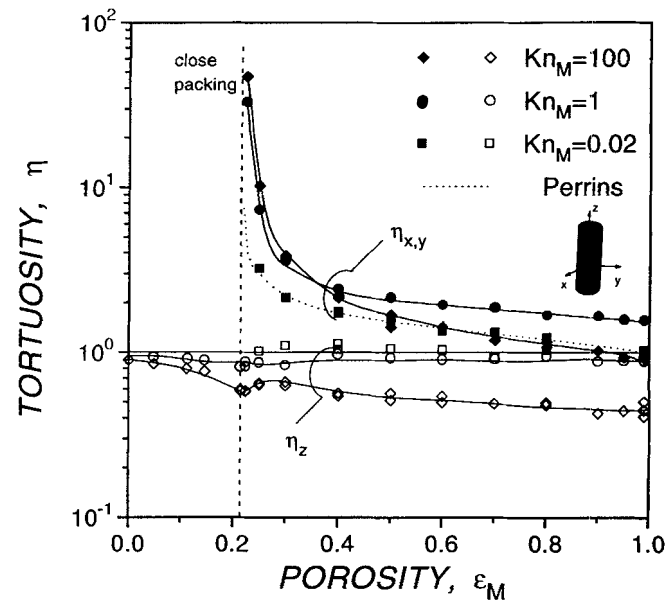

Figure 5. Tortuosities vs. porosity for a square array of solid cylinders.

seen in the obtained diffusivities from different computational runs. The effective diffusivities have been rendered dimensionless by dividing by $\bar{v}a$. As expected, the diffusivity increases with increasing Knudsen number and increasing macroporosity. At the close-packing limit (indicated by the vertical dashed line at $\epsilon_M = 1 - \pi(r_b/a)^2 = 0.2146$), the diffusivity perpendicular to the fibers approaches zero, whereas the diffusivity parallel to the fibers still has a nonzero value, as uninterrupted paths remain available to the molecules for diffusion in that direction.

The behavior of the tortuosity factor vs. porosity is much more interesting than that of the effective diffusivities. Tortuosity values, extracted from the diffusivity data of Figures 3 and 4 by applying Eqs. 17–20 are given in Figure 5. Since for diffusion in the z direction (parallel to the cylinders), the direction of the pores and of the macroscopic concentration gradient coincide, the tortuosity factor has a value of 1 at all porosities in the bulk diffusion regime (for $Kn_M = 0.02$). The tortuosity factor for Knudsen diffusion ($Kn_M = 100$) in the same direction decreases from 0.89 at the zero porosity limit —this result can be obtained analytically, as will be explained below—to about 0.45 at high porosities. For transition regime diffusion at $Kn_M = 1$ in the z direction, the tortuosity factor is smaller than 1, having an average value of about 0.93. Much larger tortuosity factors are encountered in the other two directions in all diffusion regimes. An interesting observation for these results is that the transversal tortuosity η_{xy} for $Kn_M = 1$ is lower than that for $Kn_M = 100$ at low porosities, whereas the opposite behavior occurs at high porosities. This behavior is at variance with the results of Tomadakis and Sotirchos (1993a) for diffusion in unidirectional random filament structures (non-, partially, or fully overlapping), where it was found that the tortuosity perpendicularly to the fibers increased monotonically with the porosity and the Knudsen number in all cases.

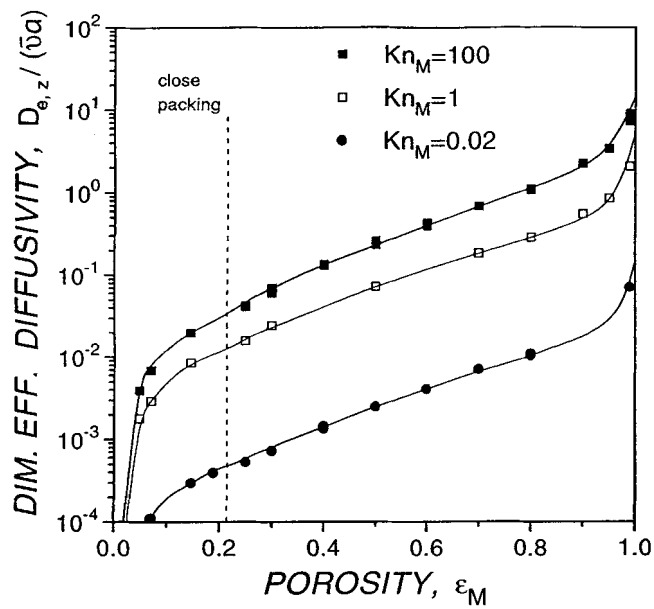

Figure 4. Dimensionless axial effective diffusivities vs. porosity for a square array of solid cylinders.

Results of the variation of the effective diffusivities and of the x or y tortuosity with the Knudsen number are shown for two values of porosity (0.25 and 0.5) in Figures 6 and 7, respectively. Figure 7 shows that there is little variation in the value of the tortuosity factor outside the [0.02, 100] Knudsen number range. The Knudsen number limits for predominantly bulk or Knudsen regime diffusion are therefore in agreement with those found by Tomadakis and Sotirchos (1993a), and thus justify our choices of 0.02 and 100 as Knudsen number values representative of bulk and Knudsen regime diffusion, respectively. For $\epsilon_M = 0.25$, the tortuosity factor increases monotonically with the Knudsen number. Similar behavior was seen in the results of Tomadakis and Sotirchos (1993a,b) for random fibers. A completely different situation

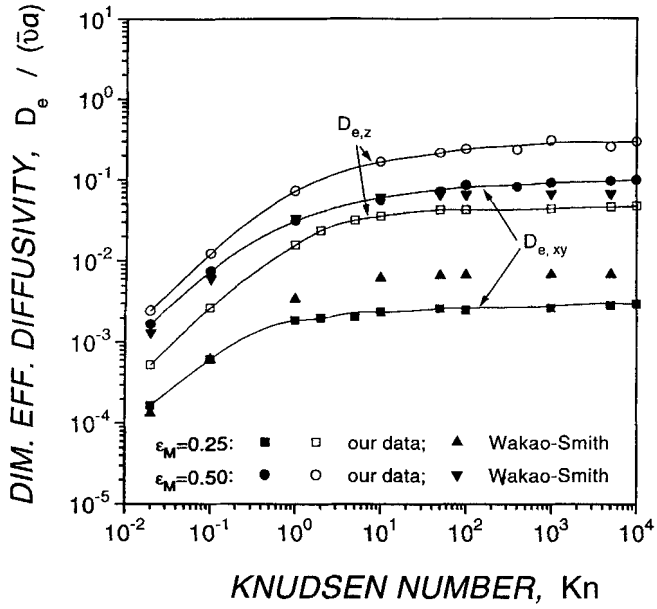

Figure 6. Dimensionless effective diffusivities vs. Knudsen number for a square array of solid cylinders for $\epsilon = 0.25$ and $\epsilon = 0.5$.

results for $\epsilon_M = 0.5$, where the tortuosity factor goes though a maximum between the bulk and Knudsen regime limits, in agreement with the results of Figure 5. This behavior is most probably a consequence of the ordered structure of a square array of cylinders, which leads to a relatively higher density of long molecular paths in the Knudsen regime in comparison to random fiber structures. The probability of finding such segments in the molecular paths decreases drastically in the transition regime, and this in turn leads to a much larger decrease in the effective diffusivity than for random fiber structures.

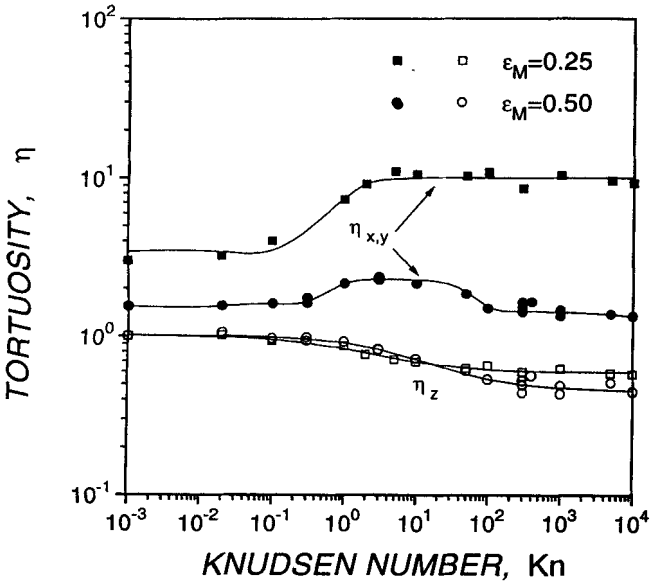

Figure 7. Tortuosities vs. Knudsen number for the cases of Figure 6.

The diffusivities in the parallel (z) and perpendicular (x or y) directions vary slowly with the Knudsen number for $Kn > 100$ (see Figure 6), but they reach a finite limit only for porosities below the close-packing limit. (Of course, in this porosity range the perpendicular diffusivity is zero for all Knudsen numbers.) It turns out that the effective diffusivity in any direction increases without limit with increasing Kn if the fibers do not overlap with each other, becoming infinitely large—and the tortuosity factor zero—for an infinite Knudsen number. This behavior cannot be inferred from the results of Figure 6 because of the relatively low rate of variation of the effective diffusivity in the high Knudsen number range. We can prove this result by using an analytical expression derived by Kennard (1938) for the Knudsen diffusivity in unidirectional pore structures.

According to this expression, the effective Knudsen diffusivity ($Kn \to \infty$) parallel to the walls of a unidirectional pore structure is given by

$$D_{e,z} = \frac{\epsilon \pi \bar{v} \bar{d}_I^c}{8}, \tag{21}$$

where $\bar{d}_I^c$ is the I-randomness (interior radiator randomness) mean chord length (Coleman, 1969) of the cross section of the porous medium (perpendicular to the pore walls), that is, the average length of a random chord drawn from a randomly chosen point in the interior of the cross section in a random direction. In conjunction with the definition of the tortuosity factor, Eq. 21 leads to the following expression for the Knudsen tortuosity:

$$\eta_z^K = \left(\frac{8}{3\pi}\right)\left(\frac{\bar{d}}{\bar{d}_I^c}\right). \tag{22}$$

For randomly overlapping cylinders, $\bar{d}/\bar{d}_I^c$ is equal to $2/\pi$, and the tortuosity factor parallel to the fibers has the value $16/3\pi^2 = 0.54\cdots$ (Tomadakis and Sotirchos, 1993a). For the square array of cylinders that we consider here, $\bar{d}_I^c$ is obviously finite for overlapping cylinders, and thus, the tortuosity factor and the effective diffusivity in the z direction reach a finite limit as $Kn_M \to \infty$. Of course, the x or y diffusivity in this range is identically equal to zero. As the porosity goes to zero, the cross section of each individual channel formed among four adjacent cylinders approaches a square, and it can be shown (using Eq. 22) that the z tortuosity factor becomes equal to $0.897\cdots$. To prove that for a square array of nonoverlapping cylinders the tortuosity factor goes to zero at the Knudsen limit for porosities larger than the close-packing limit, we can avoid dealing directly with the square array structure and use instead a result given by Coleman for the mean I-random chord length of a rectangle of sides a and b, according to which

$$\bar{d}_I^c(a,b) = \frac{2}{3\pi ab}\left\{a^3 + b^3 - r^3 + 3ab\left[a\ln\left(\frac{b+r}{a}\right) + b\ln\left(\frac{a+r}{b}\right)\right]\right\}, \tag{23}$$

with $r=\sqrt{a^2+b^2}$. As the aspect ratio of the rectangle goes to infinity (i.e., as a slit-shaped pore is obtained), it can be shown using Eq. 23 that $\bar{d}_I^c$ increases without limit and the tortuosity factor for diffusion in directions parallel to the pore walls goes to zero. A structure consisting of infinite aspect-ratio (slit-shaped) pores can be obtained from a square array by replacing each row of cylinders in a certain direction by a solid lamina whose thickness equals the cylinder diameter. Obviously, an I-random chord on a cross section of the laminated structure is smaller or equal to the I-random chord that is generated on the corresponding cross section of the square array of cylinders using the same radiator point and the same direction. This implies that $\bar{d}_I^c$ for a square array of cylinders is infinitely large in all directions, and therefore the effective diffusivity for $Kn_M \to \infty$ is infinitely large as well.

Perrins et al. (1979) derived an equation for the estimation of the effective transversal transport conductivity of a structure consisting of cylinders of conductivity $D_{c,xy}$ arranged in a regular array (square or hexagonal) and embedded in a matrix of transversal conductivity $D_{m,xy}$, at the limit of continuum transport in each phase. Their result for the effective conductivity perpendicular to cylinders arranged in a square array is

$$\frac{D_{e,xy}}{D_{m,xy}} = 1 - \frac{2f}{T + f - \dfrac{0.305827f^4T}{T^2-(1.402958f^8)} - \dfrac{0.013362f^8}{T} + \cdots}, \tag{24}$$

$$\sigma = \frac{D_{c,xy}}{D_{m,xy}}; \qquad T = \frac{1+\sigma}{1-\sigma}; \qquad f = 1-\epsilon, \tag{25}$$

where ϵ is the volume fraction of the matrix. As with the cylinders, the effective diffusivity is given by the law of mixtures:

$$\frac{D_{e,z}}{D_{m,z}} = (1-\epsilon)\frac{D_{c,z}}{D_{m,z}} + \epsilon. \tag{26}$$

Equation 24 was applied to continuum (bulk) diffusion in the pore space of a square array of solid cylinders by setting $D_{m,xy} = ((1/3)\bar{\lambda}\bar{v})/(\bar{v}a)$ and $D_{c,xy} = 0$. The obtained results were found to be in excellent agreement with the simulation data of Figure 5.

A frequently used equation to estimate transition regime diffusivities from the Knudsen and bulk limit values is the so-called Bosanquet formula (Pollard and Present, 1948), according to which

$$\frac{1}{D_{e,j}} = \frac{1}{D_{e,j}^b} + \frac{1}{D_{e,j}^K} \tag{27}$$

$$\eta_j = \frac{\eta_j^b + \eta_j^K Kn}{1+Kn}. \tag{28}$$

Subscript j denotes x-, y-, or z-directional diffusivities, and superscripts b and K are used to denote bulk and Knudsen regime properties, respectively. Tomadakis and Sotirchos (1993a) found that the Bosanquet formula offered satisfactory approximation for the transition regime diffusivities in all fibrous structures they considered (1-, 2-, or 3-directional, partially (1-directional), or freely overlapping), the only exception being parallel to the fibers of unidirectional structures. It is obvious from the results of Figure 5—where the transition regime tortuosities do not always lie between those for bulk and Knudsen diffusion—that for a square array this formula also fails perpendicular to the cylinders. This result is most probably a reflection of the regularity of this structure and of the divergence of the effective diffusivity at the Knudsen limit. It should be pointed out that when the actual value $D_{e,j}^K = \infty$ is used in Eqs. 27 and 28 instead of the finite value at $Kn_M = 100$, the predicted transition diffusivity is equal to the bulk value and the tortuosity factor becomes $\eta_j^b/(1+Kn)$. (Kn and Kn_M denote the same variable for a structure of solid bundles.)

Square array of filament bundles

A regular array of filament bundles represents one of the simplest structures that exhibit two length scales associated with wall-to-wall distances in the pore space. Our literature search uncovered no studies on diffusion of gases in such inhomogeneous periodic structures. Results for square arrays of filament bundles are presented and discussed in this section in three groups of figures, one for each regime of diffusion (Knudsen, transition, and bulk). The effective diffusivities are reported in dimensionless form. The reference diffusivity is chosen again as $\bar{v}a$, and in this way, results obtained for different r_f/r_b ratios or intrabundle porosities are directly comparable with those obtained for a square array of solid cylinders. The abscissa in each figure is the interbundle porosity ϵ_M, and a vertical dashed line is used to indicate the close-packing interbundle porosity ($\epsilon_M = 0.2146$) for a square array of cylinders. Values of ϵ_M lower than 0.2146 correspond to partially overlapping bundles, a structure representative of unidirectional fibrous preforms in which the bundles are pressed against each other. A zero value of ϵ_M corresponds to a homogeneous structure of randomly overlapping fibers like the ones recently investigated by Tomadakis and Sotirchos (1991a, 1993a). The dotted lines in each graph are those for a square array of solid cylinders ($\epsilon_\mu = 0$), discussed in the previous section. The solid curves are curves fitted to the simulation data, unless otherwise stated.

Knudsen Regime. The factors affecting the Knudsen diffusivity in the type of structures we examine are the interbundle porosity ϵ_M, the intrabundle porosity ϵ_μ, and the ratio of characteristic lengths of the two spaces (intrabundle and interbundle) r_f/r_b. As in the case of square arrays of solid cylinders, the value of the effective diffusivity is infinite in all directions at $Kn \to \infty$ for interbundle porosities above the overlapping limit. Thus, when reference is made to diffusion in the Knudsen regime for such structures, we refer to the regime where the effective diffusivity varies slowly with the Knudsen number. The results we present are for $Kn_M = 100$ if $\bar{d}_M > \bar{d}_\mu$. For macroporosities close to zero, where the interbundle characteristic length becomes smaller than $\bar{d}_\mu$, the presented results are for $Kn_\mu = 100$.

Results on the effect of intrabundle porosity on the effective directional diffusivities (constant r_f/r_b), are shown in Figure 8, and the influence of the r_f/r_b ratio is examined in Figure 9 (constant ϵ_μ). The effective diffusivities shown in

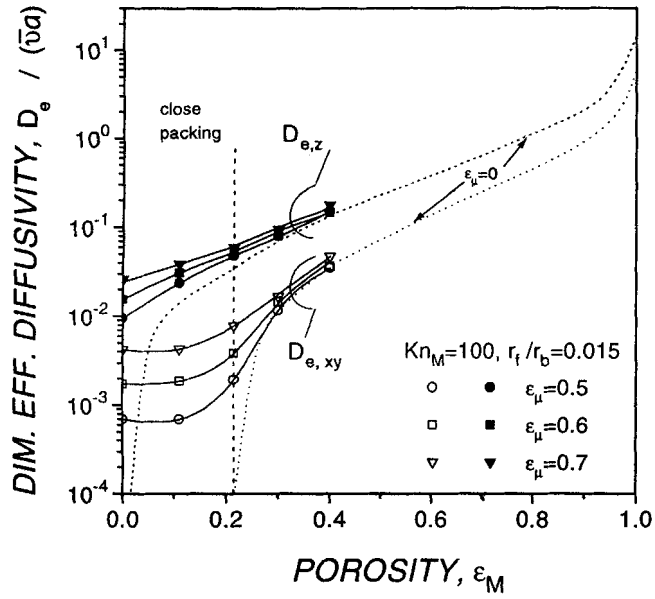

Figure 8. Dimensionless effective diffusivities vs. macroporosity for Knudsen diffusion in a square array of filament bundles with characteristic length ratio $r_f/r_b = 0.015$ for various values of microporosity.

Dotted curves represent data for an array of solid cylinders for $Kn_M = 100$.

Figure 8 are for r_f/r_b equal to 0.015, but qualitatively similar results are obtained for other values of the characteristic length ratio. The effective diffusivities for $\epsilon_M \to 0$ are in agreement with those found from the results of Tomadakis and Sotirchos (1991a,b) using r_f values calculated for $(r_b/a) \simeq \sqrt{2}/2$ (half of the diagonal of the unit cell). In both figures the effective diffusivities for diffusion perpendicular to the bundles (x or y direction) are lower than those for diffusion parallel to the bundles (z direction) in all cases. For overlapping bundles ($\epsilon_M < 0.2146$), the intrabundle porosity appears to be the most important factor influencing the effective diffusivity on the (x,y) plane. As the interbundle space disappears, the behavior of the bundle structure approaches that for Knudsen diffusion in a unidirectional, random fiber structure. For a given r_f/r_b ratio, the rate of change of the effective diffusivity $D_{e,xy}$ with ϵ_M in the vicinity of the close-packing value increases with decreasing intrabundle porosity. For $\epsilon_M > 0.4$, the interbundle porosity becomes for all practical purposes the only factor affecting the diffusion process, and the x or y effective diffusivities start to approach the Knudsen diffusivities (dotted line) for a square array of solid cylinders ($\epsilon_\mu = 0$; $Kn_M = 100$). The same qualitative behavior is exhibited for diffusion parallel to the fibers, the only difference being that the effective diffusivity changes significantly with the interbundle porosity even as the value of the latter approaches zero. This behavior is a consequence of the fact that in this direction transport in the interbundle space occurs in parallel with that in the intrabundle space, and it thus retains its importance even as $\epsilon_M \to 0$.

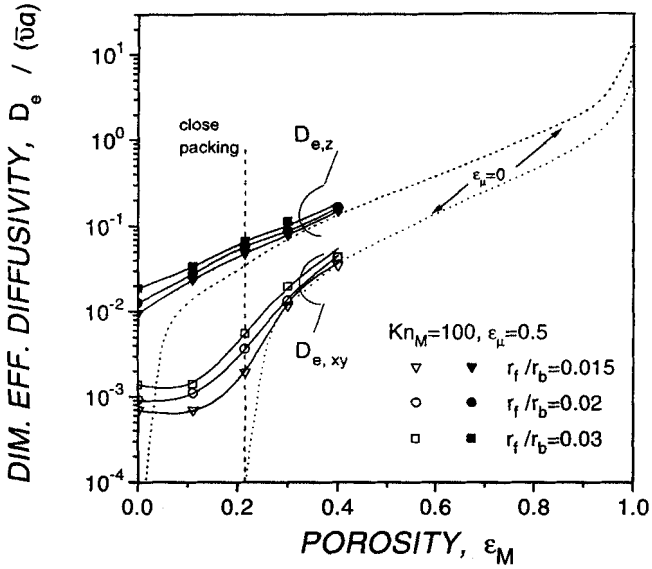

Figure 9. Dimensionless effective diffusivities vs. macroporosity for Knudsen diffusion in a square array of filament bundles for microporosity $\epsilon_\mu = 0.5$ and various values of characteristic length ratio.

Dotted curves represent data for an array of solid cylinders for $Kn_M = 100$.

Figure 9 shows that an increase in the r_f/r_b ratio increases the effective diffusivity in all directions. This effect is stronger perpendicularly to the filaments, and this is also true for the analogous effect of ϵ_μ in Figure 8. Larger r_f/r_b ratios lead to smaller diffusion resistance in the intrabundle space, and thus facilitate the diffusion process in the whole structure. Results similar, in a qualitative sense, to those of Figure 9 are obtained at intrabundle porosities larger than 0.33. For $\epsilon_\mu < 0.33$, the intrabundle structure becomes inaccessible perpendicularly to the filaments (Burganos and Sotirchos, 1989), and the gas molecules cannot travel through the intrabundle space in the x or y direction. As a result, the diffusivity perpendicular to the filaments is the same as the value for an array of solid cylinders of the same radius. On the other hand, transport parallel to the filaments is possible at all intrabundle porosity values, and therefore the effective diffusivity in that direction is greater than that for solid cylinders, even for porosities below the close-packing limit (viz., $\epsilon_M < 0.2146$).

Transition and Bulk Regimes. Results for the transition regime are presented as effective diffusivities vs. interbundle porosity in Figure 10 for three values of r_f/r_b for Knudsen number $(\bar{\lambda}/\bar{d})$ equal to 100. This choice of Knudsen number leads to transition regime diffusion in the interbundle space ($5 < Kn_M < 25$) and Knudsen diffusion in the intrabundle space ($Kn_\mu > 100$) (see Eqs. 12 and 13). As a result, at the limit of zero macroporosity, the effective diffusivity values are the same as those in Figure 8 for Knudsen diffusion. The results of Figure 10 behave qualitatively in a similar manner as those of Figures 8 and 9 for Knudsen diffusion ($Kn_M = 100$). (The dotted curves shown in the figure are the diffusivities for an array of solid cylinders for $Kn_M = 100$.) Since diffusion in the micropore space occurs in the Knudsen regime at all macroporosities for $Kn = 100$, significant quantitative differences between the Knudsen and the transition regime results are observed only for high interbundle porosities, where diffusion in the interbundle space plays the most im-

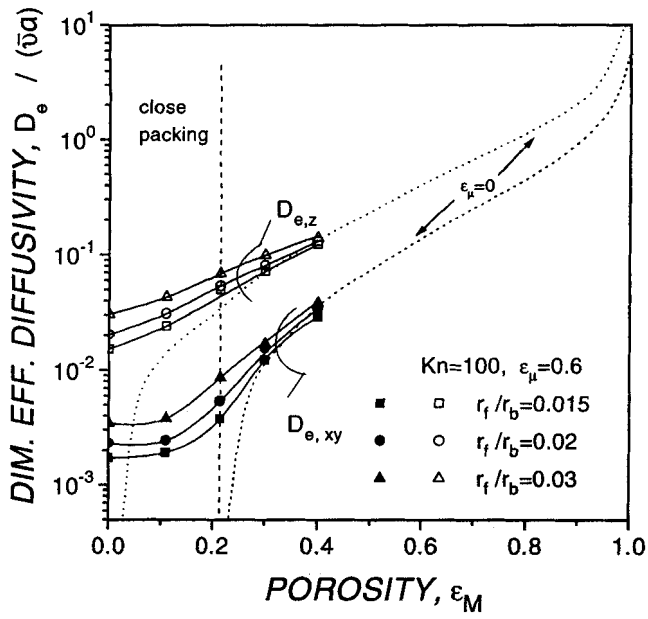

Figure 10. Dimensionless effective diffusivities vs. macroporosity for a square array of filament bundles for constant intrabundle porosity ($\epsilon_\mu = 0.6$) and various values of characteristic length ratio.

Dotted curves represent data for an array of solid cylinders for $Kn_M = 100$.

portant role. Comparison of the effective computed transition regime diffusivities with those calculated from the Bosanquet formula (Eq. 28) revealed a trend of increasing deviation between the two sets of values with increasing microporosity.

Since the bulk diffusion coefficient depends only (for sufficiently small r_f/r_b values) on ϵ_M and ϵ_μ, the bulk diffusion results are presented in Figure 11 as tortuosity factors vs. interbundle porosity with the intrabundle porosity as a parameter. Directional tortuosities for a square array of solid bundles are also shown in the same figure for comparison. As explained earlier, the mean free path for the molecules was chosen small enough to ensure that molecule–wall collisions would be much more frequent than intermolecular collisions, both between and within the bundles. For intrabundle porosities below 33% (e.g., for $\epsilon_\mu = 0$) the perpendicular tortuosity becomes infinite at the close-packing limit because of the overall inaccessibility of the structure, whereas a finite tortuosity is obtained for values above the percolation threshold. The parallel tortuosity remains almost constant at an average value of 1, in agreement with what is expected from Eq. 26. For constant total porosity, the perpendicular tortuosity in the bulk regime increases with increasing intrabundle porosity, but for ϵ_M and ϵ_μ away from their corresponding threshold values, this increase is rather small; for example, about 6% for $\epsilon = 0.7$ as ϵ_μ changes from 0.4 to 0.6.

The variation of the effective diffusivities and of the tortuosity factors with the Knudsen number is presented in Figures 12 and 13, respectively, for one of the structures we studied ($\epsilon_M = 0.4$; $\epsilon_\mu = 0.6$; $r_f/r_b = 0.02$). For both directions, parallel and perpendicular to the bundles, the effective diffusivity varies with the Knudsen number in the same way as the effective diffusivity in arrays of solid bundles (Figure 6). However, this is not the case for the tortuosity factor vs. Knudsen number curves. Comparison of Figures 7 and 12 shows that, whereas the tortuosity factor for arrays of solid bundles (perpendicular to the bundles) increases with the Knudsen number or presents a maximum in the transition regime, the tortuosity factor for arrays of filament bundles decreases sharply with the Knudsen number in the transition regime, by almost one order of magnitude in the z-direction. This behavior is caused by the fact that the characteristic pore diameter that is used to determine the reference diffusivity in the definition of the tortuosity factor for filament bundles, $\bar{d}$,

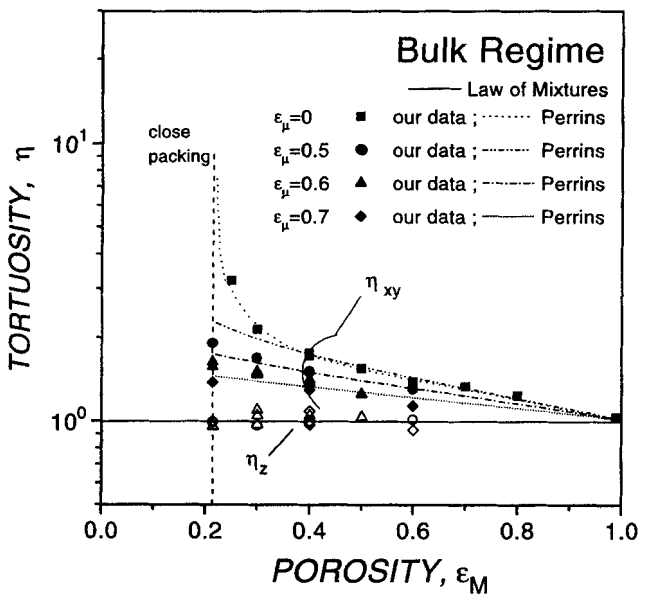

Figure 11. Tortuosities vs. macroporosity for bulk diffusion in a square array of filament bundles.

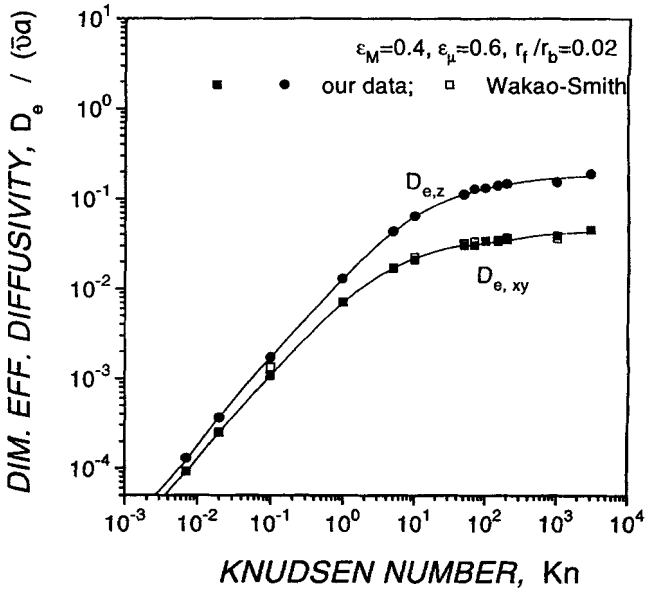

Figure 12. Dimensionless effective diffusivities vs. Knudsen number for a square array of filament bundles.

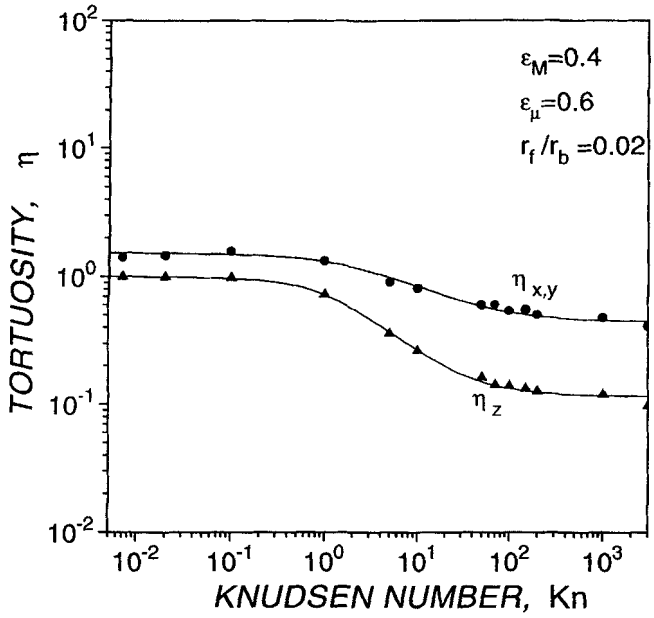

Figure 13. Tortuosities vs. Knudsen number for a square array of filament bundles.

is of the same order of magnitude as the micropore characteristic length (see Eq. 14), whereas the diffusion process in the transition and Knudsen regimes for nonoverlapping bundles is primarily influenced by transport in the interbundle space.

Comparison with analytical results

Equations 24 and 26 can be used to find the effective diffusivities in a square array of cylinders if diffusion can be treated as a continuum process both in the cylinders and in the matrix. For an array of filament bundles, this is the case in the matrix (interbundle space) if diffusion occurs in the bulk regime. Within the bundles, the characteristic diffusion length, $\bar{l}_\mu$ (see Eq. 20), varies from $\bar{d}_\mu$ in the Knudsen regime to $\bar{\lambda}$ for $\bar{\lambda} \ll \bar{d}_\mu$. $\bar{d}_\mu$ is of the order of the filament size, and therefore, for the typical case of small r_f/r_b ratios, diffusion in the bundles may be treated in all diffusion regimes as a pseudocontinuum process with effective diffusivities equal to those of a random structure of unidirectional filaments. Thus, the effective diffusivities of a square array of filament bundles for the last three cases of Table 1 (where macropore diffusion is in the bulk regime) can be approximately determined from Eqs. 24 and 26 using $\bar{\lambda}\bar{v}/3$ for the matrix diffusivity in all directions and setting the cylinder diffusivity equal to the diffusivity of a structure of randomly overlapping filaments for the prevailing value of Kn_μ. Needless to say, this can also be done for bundles consisting of nonoverlapping, partially overlapping, or even twisted filaments.

We applied the preceding procedure to the case where diffusion occurs in the bulk regime both in macropores and micropores, and very good agreement was observed between computed and predicted diffusivities, with the latter being systematically lower by about 5% on the average. We believe that the reason for this difference is that in the simulated diffusion process, molecules that do not penetrate deep in the intrabundle structure sense a lower resistance to diffusion in this region than other molecules. On the other hand, the derivation of Eqs. 24 and 26 is based on the assumption of continuum transport in both phases, and therefore the resistance that a molecule encounters in its transport in the intrabundle space is the same no matter how much time it spends there.

Equation 24 was also used to get an analytical estimate of the perpendicular effective diffusivity in the first three regimes of Table 1, where transport in the intrabundle space occurs in the Knudsen or transition regime. To do so, an equivalent perpendicular matrix diffusivity was first estimated as the matrix diffusivity that must be used in Eq. 24 for $D_{c,xy} = 0$ to find an effective diffusivity equal to that for the square array of solid cylinders at the same conditions (same Kn_M). The effective diffusivity for the array of permeable bundles was then found from Eq. 24 by using the preceding value as matrix diffusivity and the perpendicular effective diffusivity for a random, unidirectional filament structure (at the prevailing value of Kn_μ) as cylinder diffusivity. The computed values of diffusivity were found to be higher than the ones obtained from our simulations by $\simeq 15\%$ (Transvalidou, 1996).

A frequently used expression in the literature for the estimation of effective diffusivities in bidisperse structures is the Wakao–Smith model (Wakao and Smith, 1962). This model was developed for catalyst pellets (such as alumina) containing a bidisperse pore system and represented as a random assemblage of small microporous particles. Transport through the bidisperse structure was assumed to occur through three parallel routes: (1) transport through macropores of cross-sectional area fraction ϵ_M^2; (2) transport through microporous particles of cross-sectional area fraction $(1-\epsilon_M)^2$; and (3) transport through a series arrangement of macropores and microporous particles of cross-sectional area fraction $2\epsilon_M(1-\epsilon_M)$. The resulting expression for the effective diffusivity is

$$D_e = D_M\epsilon_M^2 + (1-\epsilon_M)^2\epsilon_\mu^2 D_\mu + 4\epsilon_M(1-\epsilon_M)\frac{1}{1/D_M + 1/\left(\epsilon_\mu^2 D_\mu\right)}, \quad (29)$$

where D_M and D_μ are the macropore and micropore diffusivities, respectively, obtained from the equations (Bosanquet formula)

$$\frac{1}{D_M} = \frac{1}{D^b} + \frac{1}{D_M^K} \quad (30)$$

$$\frac{1}{D_\mu} = \frac{1}{D^b} + \frac{1}{D_\mu^K}, \quad (31)$$

where D^b is the bulk diffusivity $(1/3\bar{\lambda}\bar{v})$ and D^K is the Knudsen diffusivity for a single pore $(1/3(\bar{d}_M$ or $\bar{d}_\mu)\bar{v})$. Obviously, D^b and $D^K_{(M \text{ or } \mu)}$ are the reference diffusivities (see Eqs. 17–19) used to define tortuosity factors in the bulk and Knudsen diffusion regimes, respectively, and $D_{(M \text{ or } \mu)}$ is the reference diffusivity in the transition regime. Therefore, the Wakao–Smith model predicts tortuosity factor $1/\epsilon_M$ for diffusion in the macropore space and $1/\epsilon_\mu$ for diffusion in the filament bundles.

Equation 29 can be applied to the square array of fiber bundles in the perpendicular direction. Parallel to the fibers,

there are only two routes of mass transport, through the bundles and through the macropores, and an equation analogous to the law of mixtures (Eq. 26) results when the procedure used for the derivation of Eq. 29 is followed:

$$D_{e,z} = D_M \epsilon_M + (1 - \epsilon_M)\epsilon_\mu D_\mu. \tag{32}$$

This equation predicts tortuosity factors equal to 1 in all diffusion regimes, and it thus tends to underpredict the effective diffusivity in the Knudsen and bulk diffusion regimes.

Diffusivity values predicted by the Wakao–Smith model are presented in Figure 12. It is seen that for the particular structure examined in this figure, Eq. 29 provides an excellent approximation to the perpendicular effective diffusivity over the whole Knudsen number range. Application to other structures showed that the Wakao–Smith approximation overpredicted the effective diffusivity in the lower end of the interbundle and intrabundle porosity ranges. For the intrabundle porosity, this may be seen in Figure 6, where diffusivity values predicted by the Wakao–Smith model for an array of solid cylinders are shown along with the simulation data. The failure of the Wakao–Smith equation as the percolation thresholds of the interbundle and intrabundle regions are approached is hardly surprising considering that the tortuosity factor it predicts in each region diverges to infinity at zero porosity and not at the percolation threshold.

In many applications, the Wakao–Smith model is simplified by assuming that diffusion through the microparticles is the controlling step for diffusion through a series arrangement of macropores and microparticles (bundles in our case). Use of the simplified equation, namely,

$$D_e = D_M \epsilon_M^2 + (1 - \epsilon_M)(1 + 3\epsilon_M)\epsilon_\mu^2 D_\mu \tag{33}$$

gives results comparable to those of the complete model (Eq. 29) in the Knudsen regime and the upper end of the transition regime, but overestimates significantly the effective diffusivity in the bulk diffusion regime where the diffusion resistances through the interbundle and intrabundle spaces are comparable.

Summary

In many applications where fibrous media are encountered, it is necessary to know the effective diffusivities of fluid species through the pore space of these materials in order to be able to analyze and study the occurring processes. Several studies have been presented in the literature on diffusion through fibrous media, whose constituent elements (fibers or filaments) are uniformly distributed in space. However, many of the fibrous structures used in applications possess more than one level of structural organization, that is, the fibers or filaments are grouped into independent structures (threads or tows for woven media), which are subsequently organized into the final structure or into another substructure. In a first attempt to investigate the effects of structural organization on the transport properties of fibrous media, we investigated the problem of gaseous diffusion in the Knudsen, transition, and bulk regimes in square arrays of filament bundles, of cylindrical cross section, consisting of unidirectional, freely overlapping cylindrical filaments. Effective diffusion coefficients were computed using a stochastic simulation method based on the computation of the mean square displacement of a large number of molecules (random walkers) diffusing in the pore space. Effective diffusivities were also computed for square arrays of solid cylinders, and the obtained values were compared with those of arrays of permeable bundles (porous cylinders).

The dependence of the effective diffusivity on filament-to-bundle-radius ratio, intrabundle porosity, interbundle porosity, and Knudsen number was investigated in detail. Fiber-to-bundle-radius ratios of 0.015, 0.02 and 0.03 were used in the computations. In the bulk diffusion regime, the tortuosity parallel to the bundles was, on the average, equal to 1 at all porosities—in agreement with the law of mixtures—whereas that in the perpendicular direction showed negligible dependence on the fiber-to-bundle-radius ratio and small variation for constant total porosity, as the intrabundle and interbundle porosities changed for values larger than their percolation thresholds. The Knudsen and transition regime diffusivities depended mainly on the fiber-to-bundle-radius ratio and the intrabundle porosity for interbundle porosities close to and below the percolation threshold of the interbundle space (about 0.21). Because of its relatively high mass-transport resistance, transport in the intrabundle space controlled the overall transport process below the percolation threshold of the interbundle structure, but its contribution was rather insignificant for interbundle porosities above 50%.

The computed diffusivities were compared to the predictions of a number of analytical or semianalytical formulas. By treating the transport processes in the intrabundle and interbundle spaces as pseudocontinuum and using the simulation results of Tomadakis and Sotirchos (1993d) for unidirectional filament structures and our results for square arrays of solid cylinders to determine effective diffusion coefficients for these processes, we were able to use an analytical expression derived by Perrins et al. (1979) for square arrays of conductive cylinders in a conductive matrix to obtain analytical estimates for the effective diffusivities in square arrays of filament bundles. In the bulk regime, the estimated diffusivities were found to be lower by about 5% than the simulation results, whereas the opposite trend was observed, in general, in the Knudsen regime, with the differences being as large as 15%. The simulation results were compared with the predictions of the diffusivity expression for the bidisperse structures of Wakao and Smith (1962). Since this expression predicts zero percolation threshold for the interbundle and intrabundle structures, very good agreement was observed only toward the high-porosity range, away from the percolation thresholds of the two substructures. The reciprocal additivity expression (Bosanquet formula), which is commonly used to obtain transition regime diffusivities from the Knudsen and bulk limits, produced unsatisfactory estimates both for dense and permeable cylinders, even for diffusion perpendicular to the cylinders, in which direction it was found to perform well for random arrays of cylinders (Tomadakis and Sotirchos, 1993a). This different behavior is most probably due to the regular structure of the square array that makes the effective diffusivity in all directions diverge to infinity as the Knudsen number is increased without limit.

Acknowledgment

This work was supported by a research grant from the National Science Foundation. Computer time for the computations reported in the article was provided by the Pittsburgh Supercomputing Center.

Literature Cited

Beran, M. J., *Statistical Continuum Theories*, Wiley, New York (1968).

Burganos, V., and S. Sotirchos, "Knudsen Diffusion in Parallel Multidimensional or Randomly Oriented Capillary Structures," *Chem. Eng. Sci*, **44**, 2451 (1989).

Chandrasekhar, S., "Stochastic Problems in Physics and Astronomy," *Rev. Mod. Phys.*, **15**, 1 (1943).

Coleman, R., "Random Paths through Convex Bodies," *J. Appl. Probab.*, **6**, 430 (1969).

Einstein, A., *Investigations on the Theory of the Brownian Movement*, Dover, New York (1926).

Hashin, Z., and S. Shtrikman, "A Variational Approach to the Theory of the Effective Magnetic Permeability of Multiphase Materials," *J. Appl. Phys.*, **33**, 3125 (1962).

Kellerer, A. M., "Considerations on the Random Traversal of Convex Bodies and Solutions for General Cylinders," *Rad. Res.*, **47**, 359 (1971).

Kennard, E. H., *Kinetic Theory of Gases*, McGraw-Hill, New York (1938).

Ko, F. K., "Preform Fiber Architecture for Ceramic Matrix Composites," *Amer. Ceram. Soc. Bull.*, **68**, 401 (1989).

Maxwell, J. C., *A Treatise on Electricity and Magnetism*, Clarendon Press, Oxford (1881).

McAllister, L. E., and W. L. Lachman, "Multidirectional Carbon-Carbon Composites," *Handbook of Composites*, Vol. 4, A. Kelly and S. T Mileiko, eds., Elsevier, Amsterdam (1983).

Melkote, R. R., and K. F. Jensen, "Computation of Transition and Molecular Diffusivities in Fibrous Media," *AIChE J.*, **38**, 56 (1992).

Milton, G. W., R. C. McPhedran, and D. R. McKenzie, "Transport Properties of Arrays of Intersecting Cylinders," *J. Appl. Phys.*, **25**, 23 (1981).

Naslain, R., "CVI Composites," *Ceramic Matrix Composites*, R. Warren, ed., Chapman & Hall, London (1992).

Perrins, W. T., D. R. McKenzie, and R. C. McPhedran, "Transport Properties of Regular Arrays of Cylinders," *Proc. Roy. Soc. London A*, **369**, 207 (1979).

Pollard, W. G., and R. D. Present, "On Gaseous Self-Diffusion in Long Capillary Tubes," *Phys. Rev.*, **73**, 762 (1948).

Rayleigh, Lord, "On the Influence of Obstacles Arranged in Rectangular Order upon the Properties of a Medium," *Philos. Mag.*, **34**, 481 (1892).

Sahimi, M., *Flow and Transport in Porous Media and Fractured Rock*, VCH, Weinheim, Germany (1995).

Schwartz, M. M., *Composite Materials Handbook*, 2nd ed., McGraw-Hill, New York (1992).

Sotirchos, S. V., "On a Class of Random Pore and Grain Models for Gas Solid Reactions," *Chem. Eng. Sci.*, **42**, 1262 (1987).

Sotirchos, S. V., "Dynamic Modeling of Chemical Vapor Infiltration," *AIChE J.*, **37**, 1365 (1991).

Tomadakis, M. M., and S. V. Sotirchos, "Effective Knudsen Diffusivities in Structures of Randomly Overlapping Fibers," *AIChE J.*, **37**, 74 (1991a).

Tomadakis, M. M., and S. V. Sotirchos, "Knudsen Diffusivities and Properties of Structures of Unidirectional, Partially Overlapping Fibers," *AIChE J.*, **37**, 1175 (1991b).

Tomadakis, M. M., and S. V. Sotirchos, "Ordinary and Transition Regime Diffusion in Random Fiber Structures," *AIChE J.*, **39**, 397 (1993a).

Tomadakis, M. M., and S. V. Sotirchos, "Effective Diffusivities and Conductivities of Random Fibers of Non-overlapping, Partially Overlapping Unidirectional Fibers," *J. Chem. Phys.*, **99**, 9820 (1993b).

Tomadakis, M. M., and S. V. Sotirchos, "Ordinary, Transition, and Knudsen Regime Diffusion in Random Capillary Structures," *Chem. Eng. Sci.*, **48**(19), 3323 (1993c).

Tomadakis, M. M., and S. V. Sotirchos, "Transport Properties of Random Arrays of Freely Overlapping Cylinders with Various Orientations Distributions," *J. Chem. Phys.*, **98**, 616 (1993d).

Tomadakis, M. M., and S. V. Sotirchos, "Random Paths in Random Arrays of Cylinders," *Rad. Res.*, **135**, 302 (1993e).

Torquato, S., "Effective Electrical Conductivity of Two-Phase Disordered Composite Media," *J. Appl. Phys.*, **58**, 3790 (1985).

Transvalidou, F., PhD Thesis, University of Rochester, Rochester, New York (1996).

Wakao, N., and J. M. Smith, "Diffusion in Catalyst Pellets," *Chem. Eng. Sci.*, **17**, 825 (1962).

Manuscript received July 7, 1995, and revision received Feb. 16, 1996.